International Journal of Mass Spectrometry 453 (2020) 116343

Contents lists available at ScienceDirect

International Journal of Mass Spectrometry

journal homepage: www.elsevier.com/locate/ijms

Fragmentation pathways of α-pyrrolidinophenone synthetic cathinones and their application to the identification of emerging synthetic cathinone derivatives

J. Tyler Davidson [a], Zachary J. Sasiene [b], Younis Abiedalla [c], J. DeRuiter [c], C. Randall Clark [c], Glen P. Jackson [a, b, *]

[a] Department of Forensic and Investigative Science, West Virginia University, Morgantown, WV, 26506-6121, USA
[b] C. Eugene Bennett Department of Chemistry, West Virginia University, Morgantown, WV, 26506-6121, USA
[c] Department of Drug Discovery and Development, Harrison School of Pharmacy, Auburn University, Auburn, AL, 36849, USA

ARTICLE INFO

Article history:
Received 29 January 2020
Received in revised form
10 April 2020
Accepted 12 April 2020
Available online 20 April 2020

ABSTRACT

The expanding use of emerging synthetic drugs is creating a growing problem for both seized drug analysts and toxicologists because the clandestine suppliers continually tweak the chemical structures to keep one step ahead of the law. Synthetic cathinones, commonly referred to as bath salts, are a specific class of emerging synthetic drugs. These substances are derivatives of cathinone, which is the psychoactive component of the *Catha edulis* plant, commonly referred to as khat. Of the synthetic cathinone class of compounds, the α-pyrrolidinophenone synthetic cathinone derivatives stand out as one of the most abused designer drugs.

The fragmentation behavior of a series of α-pyrrolidinophenone synthetic cathinones was studied with three different ionization and fragmentation techniques to enhance the current understanding of α-pyrrolidinophenone synthetic cathinones in mass spectrometers. Gas chromatography-electron ionization-mass spectrometry (GC-EI-MS) fragmentation is commonly used by seized drug analysts, whereas liquid chromatography-electrospray ionization-tandem mass spectrometry (LC-ESI-MS/MS) is more commonly used in toxicological analyses. Direct analysis in real time mass spectrometry (DART-MS) is becoming more popular as a screening technique, especially in national laboratories. Each ionization and activation method encourage particular pathways of fragmentation, and whereas some pathways are conserved across all platforms, other pathways are unique to a particular instrument. This study combines isotope-labeling, multi-stage mass spectrometry (MS^n) and accurate mass measurements with high-resolution mass spectrometry (HRMS) to enhance the current understanding about α-pyrrolidinophenone synthetic cathinones. This manuscript provides characteristic protonated tandem mass spectrometry fragmentation pathways and the mechanistic origins of the EI-MS fragmentation observed for this class of synthetic cathinones and provides examples of how this knowledge can be applied to the identification of novel synthetic cathinones.

1. Introduction

Synthetic cathinones are phenylalkylamine derivatives designed to mimic the effects of the natural chemical cathinone, the psychoactive component of the *Catha edulis* plant, commonly referred to as khat [1]. Because of their stimulant-like pharmacological effects, cathinones belong to a larger class of drugs known as novel psychoactive substances (NPS). Synthetic cathinones are often marketed as "not for human consumption" or "bath salts" to avoid legislative restrictions that have been imposed to decrease the sale and distribution of these compounds [2,3]. Unfortunately, these labels also deceive users into believing the substances are safe, which has resulted in numerous intoxication-related deaths [4]. Reported symptoms of synthetic cathinone abuse include euphoria, hallucinations, psychosis, paranoia, agitation, violent behavior, tachycardia, acidosis, seizures and even

* Corresponding author. Department of Forensic and Investigative Science, West Virginia University, Morgantown, WV, 26506-6121, USA.
E-mail address: glen.jackson@mail.wvu.edu (G.P. Jackson).

https://doi.org/10.1016/j.ijms.2020.116343
1387-3806/

death [4,5]. In 2011, the Drug Enforcement Administration (DEA) recognized a growing trend in synthetic cathinone abuse and provisionally scheduled mephedrone, methylone, and 3,4-methylenedioxypyrovalerone (3,4-MDPV) as Schedule I controlled substances [6]. However, regulation of synthetic cathinones is difficult because the synthesis of new analogs only requires minor modifications to the generic chemical structure. The structural modifications allow the new analogs to avoid legal regulations, but potentially lead to more harmful substances entering the illicit drug market [1].

Whereas synthetic cathinones have become widely distributed designer drugs, the α-pyrrolidinophenone derivatives stand out as one of the most abused designer drugs [7]. This class of compounds includes α-pyrrolidinopentiophenone (α-PVP), 3,4-methylenedioxypyrovalerone (3,4-MDPV), α-pyrrolidinoheptanophenone (PV8), α-pyrrolidinopropiophenone (α-PPP), among others [8]. The first reported seizure of these α-pyrrolidinophenone derivatives was in Germany in 1996 [9]. The key structural element of α-pyrrolidinophenone derivatives is the pyrrolidine ring substitution to the generic synthetic cathinone structure [8]. The main types of α-pyrrolidinophenone derivatives are side chain extensions and substitution on the aromatic ring (methoxy and methylenedioxy are the most common) [8].

Synthetic cathinones are inhibitors of monoamine transporters such as the dopamine transporter (DAT) and the noradrenaline transporter (NAT), which is consistent with other stimulant compounds such as amphetamines. However, α-pyrrolidinophenone derivatives are stronger inhibitors of these systems in comparison to non-pyrrolidinophenone synthetic cathinone derivatives increasing the effectiveness of these compounds [10]. In comparison to amphetamines, synthetic cathinones generally struggle to cross the blood-brain barrier, but the increased lipophilicity of the pyrrolidine substituent allows α-pyrrolidinophenone derivatives to more easily cross the blood-brain barrier than other cathinones [8,11].

Due to the widespread analysis of α-pyrrolidinophenone synthetic cathinones, there is a need to understand the fragmentation behavior under different ionization and fragmentation conditions. The analysis of seized drugs typically employs gas chromatography-electron ionization-mass spectrometry (GC-EI-MS) to identify unknowns, whereas the toxicological community often employs liquid chromatography with electrospray ionization and tandem mass spectrometry (LC-ESI-MS/MS). A third form of ionization that is prevalent in national laboratories is direct analysis in real time (DART). Whereas DART produces both odd-electron and even-electron ions based on the experimental conditions, the fragment ion spectra from EI (odd-electron) and ESI (even-electron) are known to differ, which has been documented for a variety of synthetic cathinones [12–20].

The fragmentation behavior of α-pyrrolidinophenone synthetic cathinones has been reported throughout literature; however, rarely are the underlying fragmentation mechanisms that lead to the observed fragment ions discussed or understood [13,15,19,21–24]. Instead, the mechanism(s) are either absent, vague, or improbable [25,26]. For example, when valid mechanisms have been proposed, the lack of isotopic labeling and lack of multi-stage mass spectrometry (MS^n) limit the certainty associated with the proposed mechanisms [25]. Recently, we demonstrated the first use of isotopic labeling, multi-stage mass spectrometry (MS^n), accurate mass measurements with high-resolution mass spectrometry (HRMS) and ion spectroscopy to explain the formation of the tropylium ion (*m/z* 91) and its substituted derivatives for α-pyrrolidinophenone synthetic cathinones analyzed with ESI-MS/MS [26]. Here, we extend the study to a wider variety of α-pyrrolidinophenone synthetic cathinone structures and include fragmentation pathways accessed through radical and even-electron pathways. The generation of synthetic cathinone fragmentation pathways will assist with the mass spectral interpretation and identification of future synthetic cathinone derivatives.

2. Methods

2.1. Sample preparation

This study involved the analysis of 22 α-pyrrolidinophenone synthetic cathinones that were either purchased through Cayman Chemical (Ann Arbor, MI, USA) or synthesized in-house at Auburn University. The 11 α-pyrrolidinophenone synthetic cathinones purchased through Cayman Chemical were: α-pyrrolidinopropiophenone (α-PPP), α-pyrrolidinobutiophenone (α-PBP), α-pyrrolidinovalerophenone (α-PVP), α-pyrrolidinoheptanophenone (PV8), 4-methoxy-α-pyrrolidinopentiophenone (4-MeO-α-PVP), 3′,4′-trimethylene-α-pyrrolidinovalerophenone, 3,4-methylenedioxy-α-pyrrolidinopropiophenone (3,4-MDPPP), 3,4-methylenedioxy-α-pyrrolidinobutiophenone (3,4-MDPBP), 3,4-methylenedioxypyrovalerone (3,4-MDPV), 3,4-methylenedioxypyrovalerone-d_8 on the pyrrolidine ring (3,4-MDPV-d_8), and 2,3-methylenedioxypyrovalerone (2,3-MDPV). The 11 synthetic cathinone samples synthesized at Auburn University were: ^{13}C-α-pyrrolidinovalerophenone labeled on the carbonyl carbon (^{13}C-carbonyl carbon-α-PVP), ^{13}C-α-pyrrolidinovalerophenone labeled on the α-carbon (^{13}C-α-carbon-α-PVP), ^{18}O-α-pyrrolidinovalerophenone (^{18}O-α-PVP), α-pyrrolidinovalerophenone-d_7 labeled on the alkyl chain (α-PVP-d_7), α-pyrrolidinovalerophenone-d_8 labeled on the pyrrolidine ring (α-PVP-d_8), α-methyl-pyrrolidinovalerophenone (α-PVP-methyl group), ^{13}C-α-pyrrolidinoheptanophenone labeled on the carbonyl carbon (^{13}C-carbonyl carbon-PV8), ^{13}C-α-pyrrolidinopropiophenone on the α-carbon (^{13}C-α-carbon-α-PPP), ^{13}C-4′-methyl-α-pyrrolidinohexanophenone on the carbonyl carbon (^{13}C-carbonyl carbon-MPHP), ^{13}C-3,4-methylenedioxypyrovalerone on the carbonyl carbon (^{13}C-carbonyl carbon-3,4-MDPV), and ^{13}C-Naphyrone on the carbonyl carbon. A full characterization of the synthetic samples was performed with GC-EI-MS and nuclear magnetic resonance spectroscopy (NMR) at Auburn University to confirm the correct labeling and acceptable purity prior to shipment to West Virginia University. All samples were analyzed at a concentration of approximately 100 ppm. The samples analyzed by GC-EI-MS were dissolved in HPLC grade methanol from Fisher Scientific (Palo Alto, CA, USA). All non-deuterated tandem MS samples analyzed on the Velos Pro linear ion trap (LIT) and the Accurate-Mass quadrupole time-of-flight mass spectrometer (Q-TOF) were dissolved in a solution of 49% HPLC grade methanol, 49% distilled water and 2% acetic acid. The acetic acid was supplied by Acros Organics (Palo Alto, CA, USA). The deuterated α-pyrrolidinophenone synthetic cathinones were dissolved in HPLC grade methanol to minimize H/D exchange.

2.2. Instrumentation

2.2.1. Linear ion trap

The Thermo Scientific Velos Pro linear ion trap (LIT) mass spectrometer was mounted with a heated-electrospray ionization (HESI) source. The HESI source was operated at 50 °C with a spray voltage of 4,000 V. The nitrogen sheath gas was operated at 8 arbitrary units with a nitrogen auxiliary gas flow of 5 arbitrary units. The mass spectrometer capillary temperature was 275 °C. The scan range and normalized collision energies (NCE), which were optimized for each compound are labeled with each mass spectrum. NCE is a proprietary technology used by Thermo Scientific that involves the calibration of the applied collision energy

against a reference output voltage (i.e. 5 V) and automatically compensates for the mass-dependent optimum CID efficiency of the isolated precursor ion. A NCE of 30% at *m/z* 200 therefore uses a lower amplitude than 30% NCE at *m/z* 400. Ultra-high purity helium was used as the bath gas purchased through Matheson TRIGAS (Fairmont, WV, USA).

2.2.2. Quadrupole time-of-flight

An Agilent Technologies 6538 UHD Accurate-Mass quadrupole time-of-flight (Q-TOF) mass spectrometer was operated with both dual ESI and DART ionization sources. The DART-100 source was mounted with a Vapur® interface (IonSense, Saugus, MA, USA). The DART ion source was operated with helium reagent gas at 300 °C with a flow rate of 3.0 L/min, a grid voltage of 400 V and a needle voltage of 3,500 V. The ESI source was operated with a spray voltage of 3,500 V, nitrogen drying gas at a 300 °C and a flow rate of 5 L/min. The nebulizer flow was 30 psig. All ESI samples were collected with direct injection at a flow rate of 10 μL/min. The MS fragmentor and skimmer voltages were held at 225 V and 65 V, respectively for the ESI data collection and 150 V and 25 V, respectively for the DART data collection. The DART data collection used lower fragmentor and skimmer voltages per the recommendations of IonSense. For both ion sources, the fragmentor voltage and skimmer voltage relationship was optimized to maximize the abundance of the $[M+H]^+$ precursor. Although, some in-source CID was often visible at the optimized conditions, isolation of the protonated precursor prior to activation in the collision cell ensured that all the product ions formed in beam-type CID were from the selected precursor. The scan range and collision energies were optimized for each compound of interest and are labeled with each mass spectrum. An isolation width of 1.3 Da was used for all samples. The ultra-high purity nitrogen used for the collision gas and the ultra-high purity helium used for the DART gas were purchased through Matheson TRIGAS (Fairmont, WV, USA).

The DART samples were prepared through the deposition of 5 μL of drug standard onto the closed end of 1.5 mm x 1.8 mm x 90 mm Pyrex® glass capillaries purchased from Corning Life Sciences (Corning, New York, USA) and allowed to completely dry before analysis. DART acquisition consisted of approximately 30 s of background collection, about 5 s of sample introduction, and then the analysis of a blank capillary to account for capillary-specific background. The total length of analysis was less than 90 s per sample.

2.2.3. Single quadrupole GC-EI-MS

An Agilent Technologies 7890 GC-5977 MS with an HP-5 [(5% phenyl)-methylpolysiloxane] 30 m x250 μm x 0.25 μm column by Agilent J&W Columns was used for the GC-EI-MS analyses. The GC-EI-MS parameters were as follows: injection volume was 1 μL; injection temperature was 250 °C; split ratio was 20:1. The initial oven temperature was 80 °C (1 min hold), which was ramped to 280 °C at 15 °C/min, then held for 2 min. The carrier gas (helium) flow rate was set to 1 mL/min and the transfer line temperature was set to 280 °C. The ultra-high purity helium gas was purchased from Matheson TRIGAS (Fairmont, WV, USA). The mass spectrometer was scanned from *m/z* 50–500 at a scan rate of 1,500 Da/s after a solvent delay of 2 min. The source and quadrupole temperatures were 250 °C and 200 °C, respectively.

2.3. Data analysis

Xcalibur 2.0.0.48 software was used for the data analysis on the Velos Pro. ChemStation version C.01.01 was used for the Agilent GC-EI-MS data analysis and MassHunter Qualitative Analysis B.05.00 was used for the Agilent Q-TOF data analysis. Microsoft Excel version 14 (Microsoft, Redmond, WA, USA) and ChemDraw 16.0 (PerkinElmer, Waltham, MA, USA) were used for mass spectral plots and mass spectral fragmentation mechanisms.

2.3.1. Mass spectral interpretation and mechanisms

The proposed fragmentation pathways follow the expected lowest energy structures and are based on rational electron pushing mechanisms commonly used for the interpretation of protonated tandem MS and EI-MS data [27]. The use of isotopic labels, MS^n and HRMS allows for the structural determination of all intermediates along the proposed fragmentation pathways. Deuterium labeling is not always able to identify the specific deuterium atoms and hydrogen atoms involved in tandem MS rearrangements, but such labeling usually offers some insight into the general fragmentation behavior. Finally, the observation of protonated precursor ions (even-electron) forming odd-electron product ions was observed along minor abundance pathways, which is consistent with previous reports from Fornal [28,29].

3. Results and discussion

3.1. HESI-Velos Pro MS^n

Our previous work with α-pyrrolidinophenone synthetic cathinones involved the identification that the tropylium ion (*m/z* 91) or substituted derivative ions form through different oxygen-containing intermediates that exclusively retain the α-carbon with the corresponding loss of the carbonyl carbon as neutral CO [26]. Through this project we also discovered several fragmentation behaviors of the α-pyrrolidinophenone class of synthetic cathinones. First, we identified competitive pathways for the loss of CO and ethylene (C_2H_4) from the base peak of the tandem mass spectrum. Second, we determined that the base peak in the tandem mass spectrum is primarily formed through the loss of the neutral pyrrolidine molecule. Third, we identified that the alkyl chain length has a direct impact on not only the tropylium ion formation, but also the associated intermediate product ions. Finally, we demonstrated that the α-pyrrolidinophenone synthetic cathinone fragmentation pathways remain conserved when accounting for additional substituents.

Fig. 1a shows the MS^2 analysis of protonated α-PVP-d_8, which is deuterated around the pyrrolidine ring. The product ion spectrum indicates that the deuterium labels remain on the cleaved 1-butylidenepyrrolidin-1-ium fragment observed at *m/z* 134 and that no H/D scrambling occurs prior to fragmentation. The lone exception to this observation is the presence of the primary product ion at *m/z* 221, which must arise through the loss of HDO instead of H_2O, the latter of which occurs to a slightly lesser extent at *m/z* 222. As expected, the MS^3 product ion spectrum for the pathway *m/z* 240 → 161 → (Fig. 1b) is consistent with structures proposed for the analysis of α-PVP [26], with the *m/z* 161 intermediate product ion formed through the loss of the pyrrolidine moiety (the structure of the fragment at *m/z* 161 is also provided in Fig. 5). Fig. 1c shows the MS^3 spectrum for the pathway *m/z* 240 → 134 →, which results in secondary product ions at *m/z* 106, 105 and 92. The intermediate at *m/z* 134 likely has the structure of 1-butylidenepyrrolidin-1-ium and fragments through the loss of ethylene, an ethyl radical (C_2H_5), and propylene to form the product ions at *m/z* 106, 105, and 92, respectively.

3.2. DART/ESI-Q-TOF

Fig. 2 compares MS^2 analysis of 4-MeO-α-PVP collected using the ESI and DART ionization sources on the same HRMS instrument. The main benefit of the HRMS instrument is the ability to

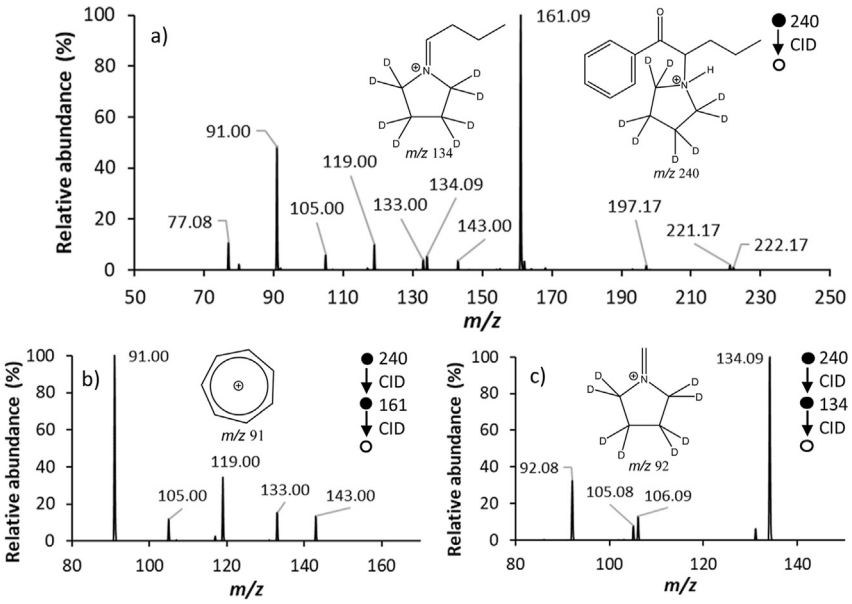

Fig. 1. Tandem mass spectra of α-PVP-d_8 on the LIT: a) MS^2 product ion spectrum of the $[M+H]^+$ molecular ion at *m/z* 240 (35% NCE); b) MS^3 product ion spectrum for the pathway *m/z* 240 → 161 → at 30% NCE showing the formation of secondary product ions at *m/z* 143, 133, 119, 105 and 91; c) MS^3 product ion spectrum for the pathway *m/z* 240 → 134 → at 30% NCE showing the formation of product ions at *m/z* 106, 105 and 92.

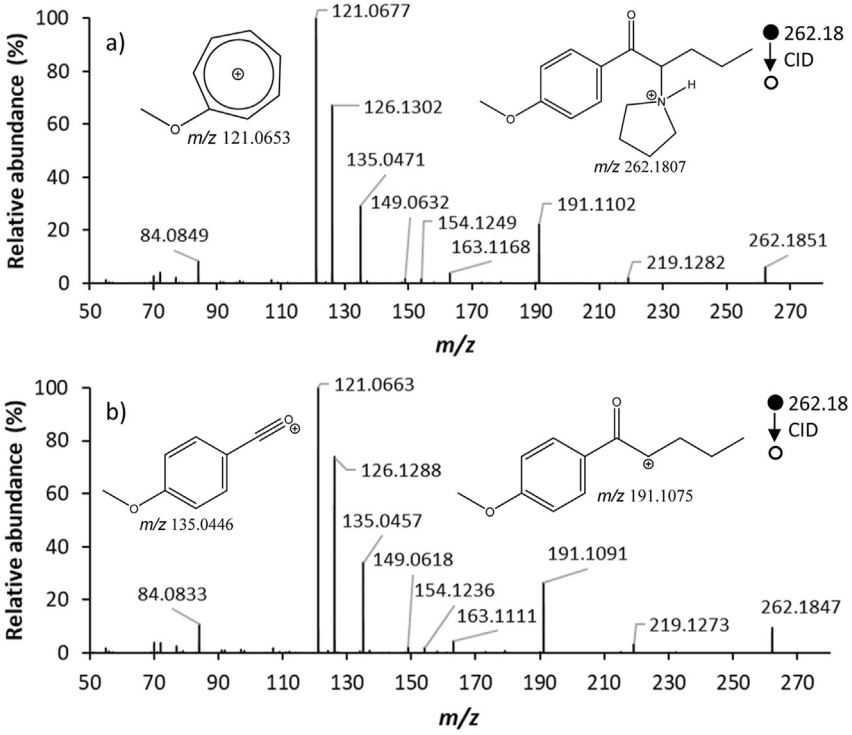

Fig. 2. Tandem mass spectra of 4-MeO-α-PVP collected on the same Q-TOF HRMS instrument using a) ESI with 25 eV collision energy and b) DART ionization with 25 eV collision energy.

determine the elemental formula of the different fragment ions. The ESI and DART mass spectra are very similar in the position and abundance of fragments, and ESI shows primary product ions at *m/z* 219.1282 (expected at *m/z* 219.1259 for $C_{13}H_{17}O_2N^{+\cdot}$; 10 ppm error), *m/z* 191.1102 (expected at *m/z* 191.1072 for $C_{12}H_{15}O_2^+$; 16 ppm error) and *m/z* 154.1249 (expected at *m/z* 154.1231 for $C_9H_{16}ON^+$; 12 ppm error). Secondary product ions at *m/z* 135.0471 (expected at *m/z* 135.0446 $C_8H_7O_2^+$; 19 ppm error) and *m/z* 126.1302 (expected at *m/z* 126.1282 for $C_8H_{16}N^+$; 16 ppm error) are observed for ESI, and they are formed via the stepwise loss of C_4H_8 and CO from the primary product ions at *m/z* 191.1102 ($C_{12}H_{15}O_2^+$) and *m/z* 154.1249 ($C_9H_{16}ON^+$), respectively. The tertiary product ion at *m/z* 121.0677 (expected at *m/z* 121.0653 for $C_8H_9O^+$; 20 ppm error) is the base peak in the ESI-generated mass spectrum. The fragment at *m/z*

121.0677 ($C_8H_9O^+$) in the ESI-generated mass spectrum arises from the loss of CO from the secondary product ion at *m/z* 149.0632 (expected at *m/z* 149.0602 for $C_9H_9O_2^+$; 20 ppm error) and the loss of propylene from the secondary product ion at *m/z* 163.1168 (expected at *m/z* 163.1122 for $C_{11}H_{15}O^+$; 28 ppm error). In all cases, the mass accuracy of both the ESI and DART mass spectra are on the order of 10 ppm from the exact masses for the proposed elemental formulas, which provides a high degree of confidence in the elemental composition of the proposed product ion structures.

Fig. 3 highlights the similarities between the MS^2 spectra from ESI and DART ionization of protonated 3,4-MDPV at *m/z* 276.1607 (expected at *m/z* 276.1599 for $C_{16}H_{22}NO_3^+$; 3 ppm error) for the ESI-generated mass spectrum. The most abundant ions appear at *m/z* 126.1305 (expected at *m/z* 126.1282 for $C_8H_{16}N^+$; 18 ppm error) and *m/z* 135.0476 (expected at *m/z* 135.0446 for $C_8H_7O_2^+$; 22 ppm error) for the ESI-generated mass spectrum, which correspond to the 1-butylidenepyrrolidin-1-ium ion and methylenedioxy-substituted tropylium ion, respectively. Due to the methylenedioxy substituent on the aromatic ring moiety, an additional dominant pathway is observed through the loss of formaldehyde (CH_2O) from fragments containing the methylenedioxy group. Ions corresponding to the loss of formaldehyde are observed at *m/z* 175.0812 (expected at *m/z* 175.0759 for $C_{11}H_{11}O_2^+$; 30 ppm error) and *m/z* 147.0821 (expected at *m/z* 147.0809 for $C_{10}H_{11}O^+$; 8 ppm error) for the ESI-generated mass spectrum, which are both 30 Da less than their predecessor ions at *m/z* 205.0922 (expected at *m/z* 205.0864 for $C_{12}H_{13}O_3^+$; 28 ppm error) and *m/z* 177.0955 (expected at *m/z* 177.0915 for $C_{11}H_{13}O_2^+$; 23 ppm error), respectively. Generally, the accurate mass measurements were on the same order of magnitude from the exact masses of the proposed elemental formula as those in Fig. 2; however, there was less agreement in the accurate mass measurements between the ESI and DART data likely due to differences in the recency of the tune prior to each analysis.

Fig. 4 compares the MS^2 spectra of protonated adducts of ^{13}C-MPHP formed by ESI and DART ionization. The labeled ^{13}C is on the carbonyl carbon in both cases. The spectra have the major structural fragments embedded. These spectra demonstrate that both ion sources produce similar mass spectra with the base peak observed at *m/z* 105.0727 (expected at *m/z* 105.0704 for $C_8H_9^+$; 22 ppm error) for the ESI-generated mass spectrum. The formation of this ion is unexpected in that the isotopically labeled carbonyl adjacent to the aromatic ring moiety must be lost prior to ring expansion, which has been previously demonstrated as a possible fragmentation mechanism of α-pyrrolidinophenone synthetic cathinones [26]. The secondary product ions at *m/z* 204.1355 (expected at *m/z* 204.1338 for $C_{12}{}^{13}CH_{17}ON^{+\cdot}$; 8 ppm error), *m/z* 190.1315 (expected at *m/z* 190.1307 for $^{12}C_{12}{}^{13}CH_{17}O^+$; 4 ppm error), and *m/z* 140.1453 (expected at *m/z* 140.1439 for $C_9H_{18}N^+$; 10 ppm error) for the ESI-generated mass spectrum originate through the loss of a butyl radical (C_4H_9), loss of the pyrrolidine molecule, and the generation of the 1-pentylidenepyrrolidin-1-ium ion, respectively. The tertiary product ions at *m/z* 134.0725 (expected at *m/z* 134.0681 for $^{12}C_8{}^{13}CH_9O^+$; 33 ppm error) and *m/z* 120.0540 (expected at *m/z* 120.0524 for $^{12}C_7{}^{13}CH_7O^+$; 13 ppm error) for the ESI-generated mass spectrum form through the loss of butylene and stepwise loss of C_5H_{10} from the primary product ion at *m/z* 190.1315 ($^{12}C_{12}{}^{13}CH_{17}O^+$). All accurate mass measurements are on the order of 10 ppm different than the exact masses for the proposed elemental formulas, which was relatively consistent throughout the Q-TOF dataset.

Fig. 5 demonstrates the proposed general pathways for the fragmentation of α-pyrrolidinophenone synthetic cathinones under protonated tandem MS conditions, where X represents substitution to the aromatic ring moiety and C_nH_{2n+1} represents varying alkyl chain lengths. Details of the ^{13}C, ^{18}O, and deuterated labeling are described in detail in Refs. [26] and are not repeated here; however, the results of the isotope-labeled compounds are entirely consistent with the pathways proposed here. The proposed

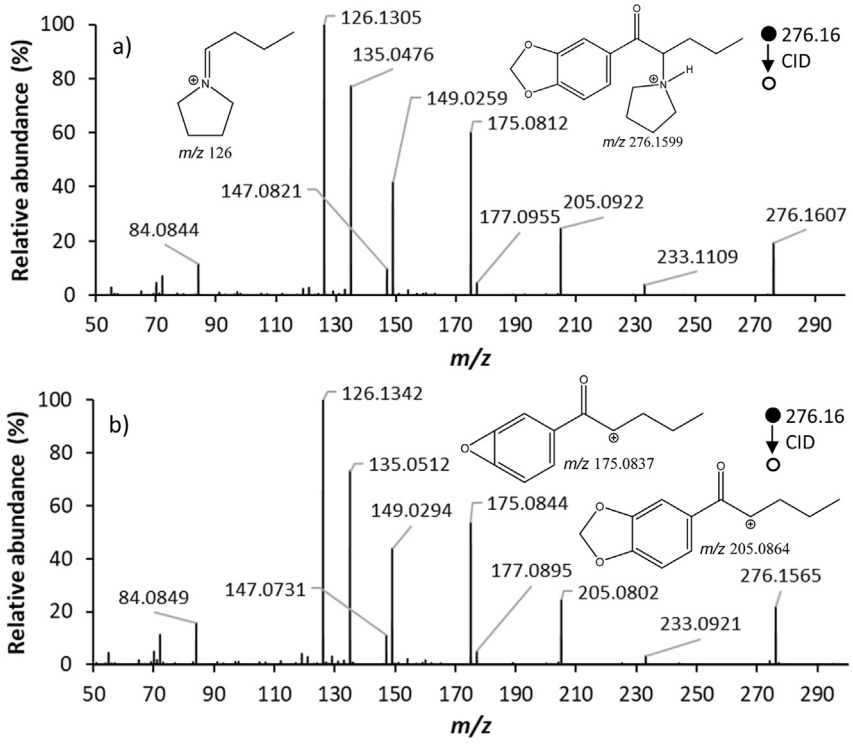

Fig. 3. Tandem mass spectra of 3,4-MDPV collected on the same Q-TOF HRMS instrument using a) ESI with a 25 eV collision energy and b) DART ionization with a 25 eV collision energy.

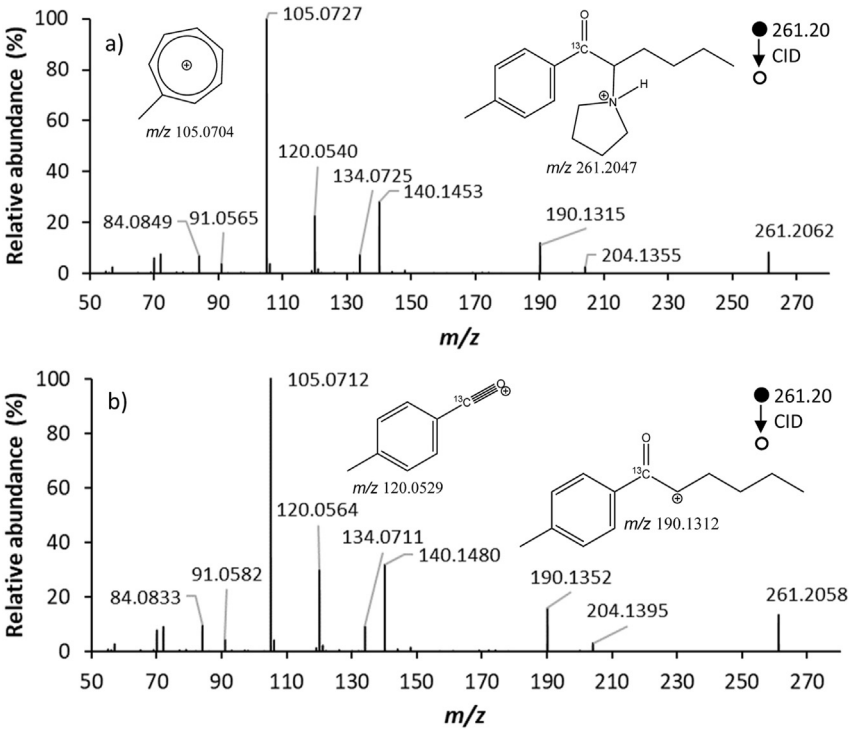

Fig. 4. Tandem mass spectra of ^{13}C-MPHP collected on the same Q-TOF HRMS instrument using a) ESI with a 25 eV collision energy and b) DART ionization with a 25 eV collision energy.

fragmentation pathways are based on data collected with both the IT and Q-TOF mass spectrometers, which are known to have differences in their fragmentation energy deposition rates. The fragmentation process with an IT mass spectrometer is considered very slow activation that occurs through 100s of collisions with the bath gas. In comparison, the Q-TOF fragmentation arises through low-energy, beam-type activation, involving 10s of collisions as the analyte passes through the collision cell [30,31]. However, in general, the mass spectra collected with both the IT and Q-TOF mass spectrometers behaved as described below in Fig. 5 with the favorability of each fragmentation pathway observed under LIT conditions indicated by the size and color of the corresponding arrow.

Based on the analysis of 21 α-pyrrolidinophenone synthetic cathinones using isotope labeling, MS^n and HRMS, the following general trends are observed. Isolation and fragmentation of the $[M+H]^+$ precursor ion typically results in primary product ions through the loss of $CH_2C_nH_{2n}$, H_2O, $C_2H_4C_nH_{n2+1}$, C_6H_6, and NC_4H_9. Of these primary product ions, the loss of NC_4H_9 (pyrrolidine molecule) is dominant, and the loss of C_nH_{2n} and H_2O are the least prevalent fragmentation pathways. The two primary product ions that produce abundant consecutive product ions are the ions at *m/z* 161, from the loss of the pyrrolidine, and *m/z* 154, from the loss of the aromatic ring, in Fig. 5. The fragmentation pathway through the intermediate at *m/z* 154 results in secondary product ions through the loss of CO (i.e. *m/z* 126) and propylene (i.e. *m/z* 112), which can then form tertiary and quaternary product ions. The fragmentation pathway through the intermediate at *m/z* 161 in Fig. 5 continues through three abundant secondary product ions at *m/z* 143, 133, and 119. The secondary product ions at *m/z* 143 and *m/z* 119 form through the loss of H_2O and propylene, respectively. However, secondary product ions at *m/z* 133 form via competing pathways through the loss of CO (28 Da) and ethylene (28 Da), as demonstrated previously [26]. The secondary product ions at *m/z* 133 in Fig. 5 fragment into tertiary product ions at *m/z* 105 and *m/z* 91. The secondary product ion at *m/z* 119 also fragment into the characteristic tropylium ion at *m/z* 91, which helps explain the significant presence of the tropylium ion in α-pyrrolidinophenone synthetic cathinones that contain at least four carbon atoms in the alkyl chain [26]. Supplemental 1 demonstrates the formation of the tropylium ion from α-PBP, α-PVP, and PV8 and the effect of alkyl chain lengths on the distribution of product ions observed in the protonated tandem mass spectra.

The biggest impact of the identification of the conserved fragmentation pathways described in Fig. 5 is the application of this information to the identification of emerging synthetic cathinones. If a questioned seized drug provides a tandem mass spectrum with an abundant neutral loss of 71 Da from the $[M+H]^+$ precursor, as well as additional peaks consistent with neutral losses of C_6H_6, $C_2H_4C_nH_{n2+1}$, H_2O and $CH_2C_nH_{2n}$, then the spectrum is consistent will all of the α-pyrrolidinophenone synthetic cathinones in this study. The presence of secondary fragmentation from any of the aforementioned peaks provides additional confidence in the identification of an α-pyrrolidinophenone synthetic cathinone.

Additionally, the ability to identify substitution to the core α-pyrrolidinophenone synthetic cathinone structure through shifts in the mass axis provides an additional tool for the identification of α-pyrrolidinophenone synthetic cathinones. Specifically, the location of the substitution can be identified based on which peaks diverge from the proposed fragmentation pathways in Fig. 5.

Table 1 shows the $[M+H]^+$ protonated precursor and the five most abundant product ions for 13 α-pyrrolidinophenone synthetic cathinones from this study. The five most abundant fragments are listed in order of decreasing abundance with all comparisons made at the same normalized collision energy in the LIT and same acceleration voltage in the Q-TOF data. These 13 standards include 11 non-isotopically labeled and two deuterated α-pyrrolidinophenone synthetic cathinones. The product ions in Table 1 highlight both the

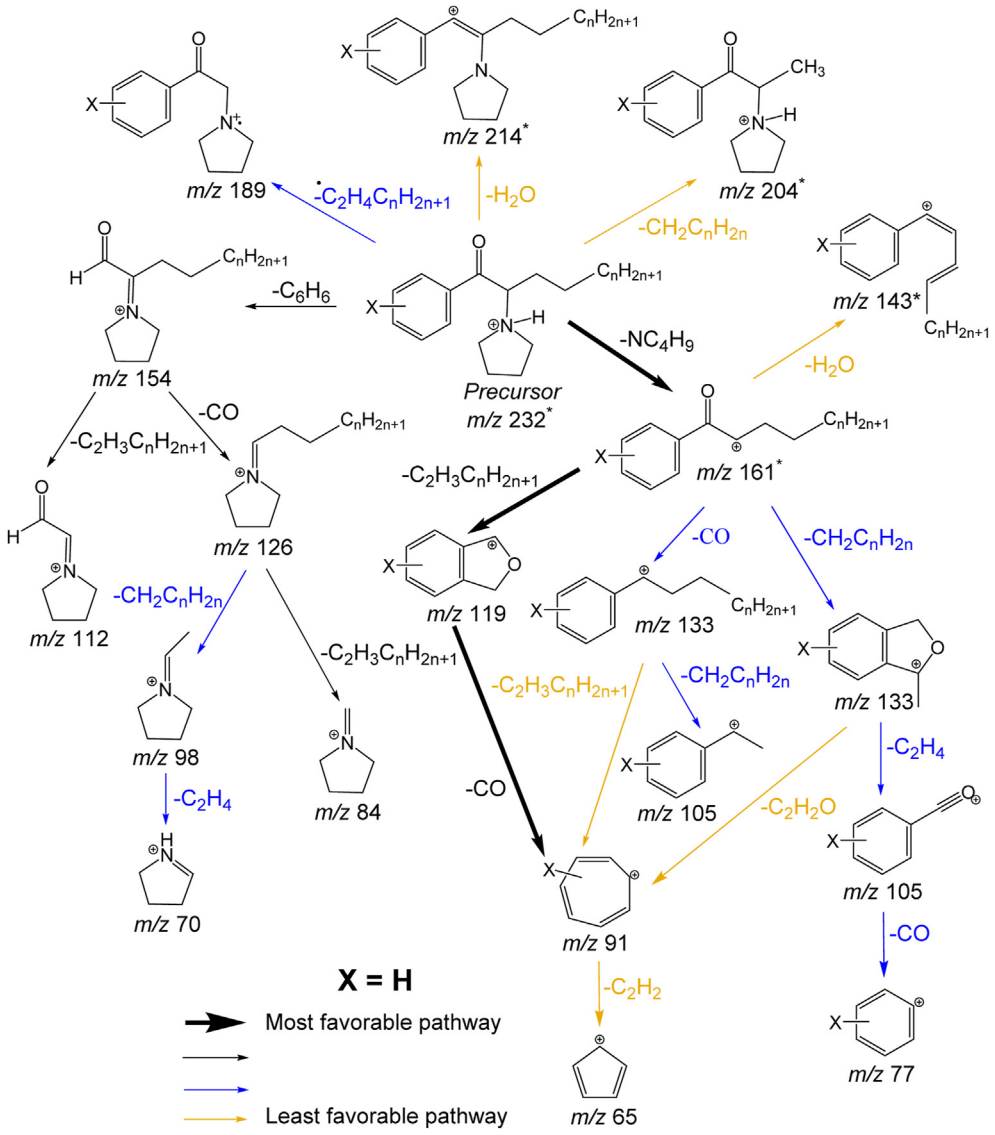

Fig. 5. Proposed general fragmentation pathways for protonated α-pyrrolidinophenone synthetic cathinones undergoing tandem MS. The model compound is α-PVP where X = H and the *m/z* values that are specific to α-PVP are indicated with an asterisk (*).

Table 1
Protonated precursor mass and the five most abundant product ions in decreasing order of abundance for 13 of the synthetic cathinones used in this study. Fragment ions are reported for both the LIT and Q-TOF instruments.

Compound	$[M+H]^+$ (*m/z*)	LIT product ions (*m/z*) @30% NCE	Q-TOF product ions (*m/z*) @25 eV
α-PPP	204	133, 105, 70, 186, 98	105.07, 98.09, 133.06, 70.06, 77.03
α-PBP	218	147, 91, 119, 70, 112	91.05, 112.11, 105.07, 70.06, 161.09
α-PVP	232	161, 91, 70, 119, 126	91.05, 126.12, 105.03, 70.06, 161.09
α-PVP-methyl	246	175, 105, 140, 72, 228	105.07, 72.08, 77.04, 140.14, 98.09
PV8	260	189, 91, 119, 107, 154	91.05, 154.16, 105.03, 70.06, 119.04
4-MeO-α-PVP	262	191, 126, 121, 163, 135	121.06, 126.12, 135.04, 191.10, 84.08
3′,4′-trimethylene-α-PVP	272	201, 131, 126, 145, 173	131.08, 201.12, 126.12, 145.06, 84.08
3,4-MDPPP	248	177, 147, 98, 149, 230	98.09, 147.04, 149.06, 177.05, 119.05
3,4-MDPBP	262	191, 161, 112, 163, 149	112.11, 161.06, 149.02, 191.07, 163.07
3,4-MDPV	276	205, 175, 126, 135, 177	126.12, 135.04, 175.07, 149.02, 205.08
2,3-MDPV	276	175, 135, 205, 177, 126	135.04, 175.07, 126.12, 149.02, 70.06
3,4-MDPV-d_8	284	205, 175, 134, 135, 177	134.17, 135.04, 149.02, 175.07, 92.13
α-PVP-d_8	240	161, 91, 77, 119, 134	91.05, 134.17, 105.03, 161.09, 77.11

frequency of occurrence for the product ions described in Fig. 5, and the similarity in fragment ion abundances between the IT and Q-TOF instruments. With the exception of the loss of formaldehyde from methylenedioxy-containing compounds, and the additional methyl group for α-PVP-methyl, the only product ion in Table 1 that is not described by Fig. 5 is *m/z* 107 for PV8 (Supplemental 1c). The

proposed elemental formula for the product ion at *m/z* 107 is $C_7H_7O^+$, which has a theoretical exact mass of *m/z* 107.0496 and is less than 5 ppm from the measured accurate mass of *m/z* 107.0490 (Supplemental 2).

3.3. GC-EI-MS

Thermal degradation was occasionally observed as shouldering or as a split peak, consistent with previous literature [32–34]; however, the formation of the 2,3-enamine degradation product was always insignificant relative to the abundance of the non-degraded parent compound. The GC-EI-MS data demonstrates that the proposed carbon backbone rearrangements observed for the protonated tandem MS data are insignificant for all compounds analyzed by EI. EI is a hard ionization source, which causes extensive fragmentation with well-established mechanisms, such as radical-directed cleavage to form the benzoylium ion at *m/z* 105. The mechanisms of fragmentation of EI-MS are both radical-directed and charge-directed, in contrast to the charge-remote 4-center eliminations that dominate the tandem mass spectra of protonated precursor ions. For example, Fig. 6a shows the GC-EI-MS spectrum of ^{13}C-α-PPP isotopically labeled with a ^{13}C on the α-carbon. The major structural fragments are embedded. The spectrum has been truncated due to the lack of high mass ions, such as the molecular ion, which is often missing with EI-MS of synthetic cathinones [14]. The presence of the benzoylium ion at *m/z* 105, phenylium ion at *m/z* 77 and the dominant 1-ethylidenepyrrolidin-1-ium ion at *m/z* 99 (accounting for ^{13}C) are all consistent with previous literature on the EI-MS fragmentation of α-pyrrolidinophenone synthetic cathinones [12,14,25,35–37].

Fig. 6b shows the truncated GC-EI-MS results for the analysis of ^{13}C-3,4-MDPV labeled with a ^{13}C on the carbonyl carbon. The major structural fragments are embedded. Even with the additional methylenedioxy substitution, the 1-butylidenepyrrolidin-1-ium ion at *m/z* 126 is the base peak of this spectrum. However, the methylenedioxy substitution does shift the phenylium and benzoylium ions by 44 Da to the observed peaks at *m/z* 121 and *m/z* 150, respectively. The product ion at *m/z* 150 accounts for the 1 Da shift for the ^{13}C present in the substituted benzoylium ion.

The truncated GC-EI-MS results for the analysis of ^{13}C-PV8 labeled with a ^{13}C on the carbonyl carbon are shown in Supplemental 3 with the major structural fragments embedded. The base peak of this spectrum is the 1-hexylidenepyrrolidin-1-ium ion at *m/z* 154, which, as expected, does not contain the ^{13}C from the carbonyl carbon. Other peaks of significant abundance are the benzoylium ion at *m/z* 106 (accounting for ^{13}C) and the phenylium ion at *m/z* 77. The conserved fragmentation pathways through the acylium and iminium ions hold true across the series of substitutions analyzed during this study.

Fig. 7 demonstrates the proposed general fragmentation mechanisms for α-pyrrolidinophenone synthetic cathinones under EI-MS conditions, where X represents substitution to the aromatic ring moiety and C_nH_{2n+1} represents varying alkyl chain lengths. The ^{13}C, ^{18}O, and deuterated labeling are not shown in these proposed general mechanisms, but were used to generate the proposed mechanisms, which are drawn explicitly for α-PVP as an example.

The two most abundant fragmentation pathways of α-

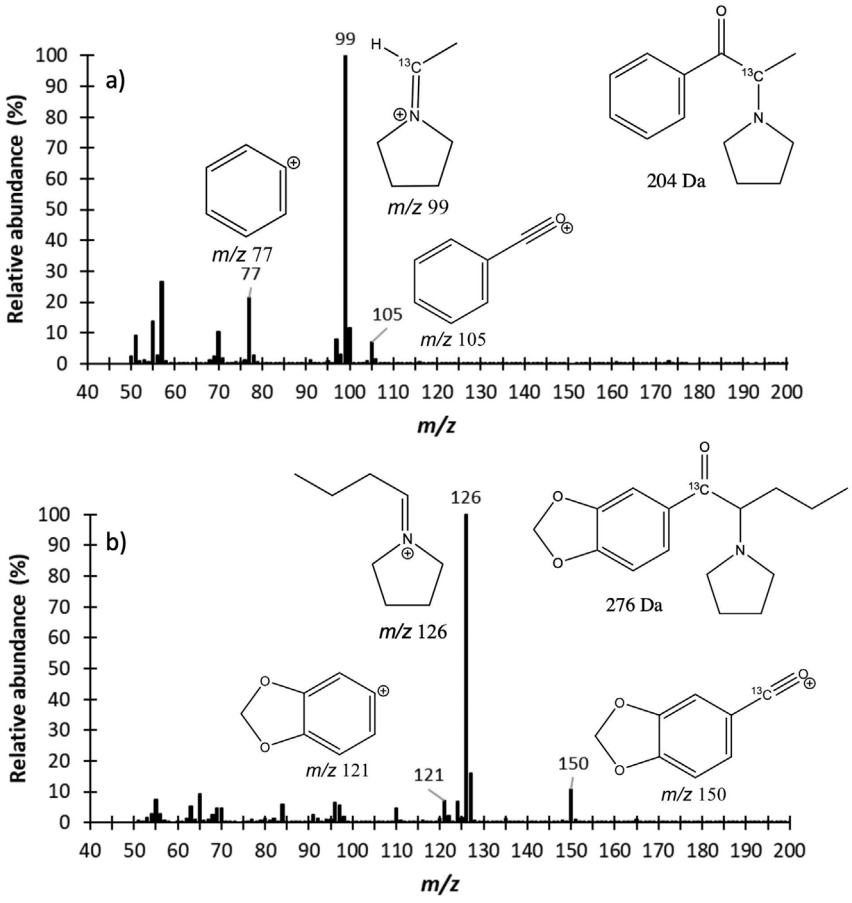

Fig. 6. Full scan mass spectra of a) ^{13}C-α-PPP and b) ^{13}C-3,4-MDPV collected with GC-EI-MS.

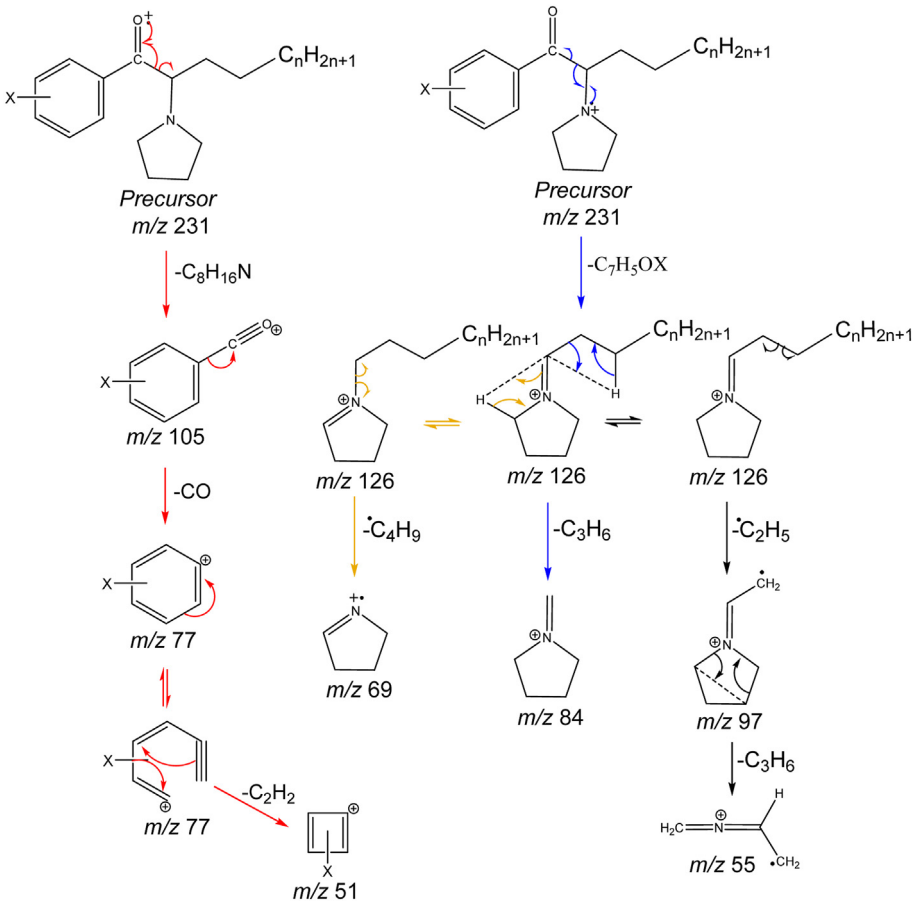

Fig. 7. Proposed general mechanisms for the fragmentation of α-pyrrolidinophenone synthetic cathinones with EI-MS (adapted from Ref. [17,25,36]). The model compound is α-PVP.

pyrrolidinophenone synthetic cathinones are acylium and iminium ions, with iminium ions being the most dominant pathway. Acylium ions form through α-cleavage initiated by a radical electron on the oxygen, which produces characteristic ions at *m/z* 105, 77, and 51 for all the α-pyrrolidinophenone synthetic cathinones studied here. However, the presence of iminium ions are far more useful for the differentiation of synthetic cathinone isomers because of the secondary and tertiary fragmentation described by Zuba [14]. The formation of the iminium ion cascade is initiated by a radical electron on the nitrogen and α-cleavage of the bond between the carbonyl carbon and the α-carbon adjacent to the pyrrolidine ring. Secondary iminium ion fragmentation forms characteristic ions, such as those demonstrated for α-PVP in Fig. 7 at *m/z* 97, 84, and 69 through the loss of an ethyl radical (˙C_2H_5), propylene, and a butyl radical (˙C_4H_9), respectively. The secondary iminium ion at *m/z* 97 further fragments into the tertiary iminium ion at *m/z* 55 through the loss of cyclopropane.

4. Conclusions

The combination of isotope-labeling, MS^n, and HRMS was used to study the fragmentation behavior of α-pyrrolidinophenone synthetic cathinones to gain a deeper understanding about the characteristic fragmentation pathways of this class of synthetic cathinone analogs. Three instruments that are common in toxicology laboratories and crime laboratories were used to develop characteristic fragmentation pathways to assist practitioners with the identification of α-pyrrolidinophenone synthetic cathinones. Through the analysis of 22 α-pyrrolidinophenone synthetic cathinones, ESI and DART ionization sources on the same Q-TOF mass spectrometer produced even-electron protonated molecular ions and almost indistinguishable tandem mass spectra. The fragmentation pathways are highly conserved between the LIT and Q-TOF mass spectrometers, although the multi-collisional environment of the ion trap occasionally tends to limit the extent of consecutive fragmentations relative to the Q-TOF instrument [27]. The Q-TOF therefore favored the abundant production of lower mass ions relative to the LIT instrument.

The identification of conserved tandem mass spectrometry fragmentation pathways through the loss of $CH_2C_nH_{2n}$, H_2O, $C_2H_4C_nH_{n2+1}$, C_6H_6, and NC_4H_9 from protonated molecular ions provides a series of diagnostic ions that can be used for the tandem mass spectrometry identification of α-pyrrolidinophenone synthetic cathinones. Particularly, the dominant pathways through the loss of pyrrolidine and the formation of iminium ions of varying side chain lengths provides a technique for structural elucidation through mass axis shifts due to additional substitutions to the core synthetic cathinone structure. The presence of diagnostic ions such as the tropylium ion at *m/z* 91, substituted iminium ions (i.e. *m/z* 126 vs *m/z* 112), and the phenylethyl derivative at *m/z* 105 provide key information about the length of the alkyl chain and substitutions to the aromatic ring moiety.

When GC-EI-MS is used to analyze α-pyrrolidinophenone synthetic cathinones, the fragmentation pathways are dominated by the formation of iminium and acylium ions as previously reported in literature [12,14,25,35–37]. This is expected due to the large energy deposition through 70 eV electron fragmentation resulting in direct α-cleavage fragmentation rather than the low-energy

rearrangements observed with collisional activation. However, the observed fragmentation mechanisms remain unaffected by substitutions to the core synthetic cathinone structure, which provides a rapid method for the identification of novel α-pyrrolidinophenone synthetic cathinones through known fragmentation pathway shifts along the mass axis. For example, the product ions observed at *m/z* 149 and *m/z* 121 for the GC-EI-MS fragmentation of 3,4-MDPV are 44 Da larger than the product ions at *m/z* 105 and *m/z* 77 for non-methylenedioxy substituted synthetic cathinones. This study highlights the differences between high energy radical-driven fragmentation in EI and lower energy collisional activation of protonated precursor ions. However, knowledge about the systematic tendencies of both techniques can be used to help support the identification of emerging synthetic drugs.

Declaration of competing interest

The authors declare that they have no known competing financial interests or personal relationships that could have appeared to influence the work reported in this paper.

CRediT authorship contribution statement

J. Tyler Davidson: Conceptualization, Methodology, Formal analysis, Writing - original draft, Data curation. **Zachary J. Sasiene:** Formal analysis, Writing - review & editing. **Younis Abiedalla:** Writing - review & editing. **J. DeRuiter:** Writing - review & editing. **C. Randall Clark:** Project administration, Writing - review & editing. **Glen P. Jackson:** Conceptualization, Project administration, Methodology, Writing - review & editing.

Acknowledgements

This project was supported by grant number 2018-75-CX-0033, awarded by the National Institute of Justice, Office of Justice Programs, U.S. Department of Justice. The opinions, findings, and conclusions or recommendations expressed in this publication are those of the authors and do not necessarily reflect the views of the Department of Justice.

Appendix A. Supplementary data

Supplementary data to this article can be found online at https://doi.org/10.1016/j.ijms.2020.116343.

References

[1] M.J. Valente, P. Guedes de Pinho, M. de Lourdes Bastos, F. Carvalho, M. Carvalho, Khat and synthetic cathinones: a review, Arch. Toxicol. 88 (1) (2014) 15–45, https://doi.org/10.1007/s00204-013-1163-9.
[2] A.L. Bretteville-Jensen, S.S. Tuv, O.R. Bilgrei, B. Field, L. Bachs, Synthetic cannabinoids and cathinones: prevalence and markets, Forensic Sci. Rev. 25 (2013) 7–26.
[3] K. Zaitsu, M. Katagi, M. Tatsuno, T. Sato, H. Tsuchihashi, K. Suzuki, Recently abused β-keto derivatives of 3,4-methylenedioxyphenylalkylamines: a review of their metabolisms and toxicological analysis, Forensic Toxicol. 29 (2) (2011) 73–84, https://doi.org/10.1007/s11419-011-0111-8.
[4] B.L. Murray, C.M. Murphy, M.C. Beuhler, Death following recreational use of designer drug "bath salts" containing 3,4-Methylenedioxypyrovalerone (MDPV), J. Med. Toxicol. 8 (1) (2012) 69–75, https://doi.org/10.1007/s13181-011-0196-9.
[5] K.N. Ellefsen, M. Concheiro, M.A. Huestis, Synthetic cathinone pharmacokinetics, analytical methods, and toxicological findings from human performance and postmortem cases, Drug Metab. Rev. 48 (2) (2016) 237–265, https://doi.org/10.1080/03602532.2016.1188937.
[6] Drug Enforcement Administration, Department of Justice, schedules of controlled substances: temporary placement of three synthetic cathinones into Schedule I, fed, Regist 76 (174) (2011).
[7] J.P. Kelly, Cathinone derivatives: a review of their chemistry, pharmacology and toxicology, Drug Test. Anal. 3 (2011) 439–453, https://doi.org/10.1002/dta.313.
[8] K. Zaitsu, M. Katagi, H. Tsuchihashi, A. Ishii, Recently abused synthetic cathinones, α-pyrrolidinophenone derivatives: a review of their pharmacology, acute toxicity, and metabolism, Forensic Toxicol. 32 (1) (2014) 1–8, https://doi.org/10.1007/s11419-013-0218-1.
[9] F. Westphal, T. Junge, B. Klein, G. Fritschi, U. Girreser, Spectroscopic characterization of 3,4-methylenedioxypyrrolidinobutyrophenone: a new designer drug with alpha-pyrrolidinophenone structure, Forensic Sci. Int. 209 (2011) 126–132, https://doi.org/10.1016/j.forsciint.2011.01.016.
[10] L.D. Simmler, T.A. Buser, M. Donzelli, Y. Schramm, L.H. Dieu, J. Huwyler, S. Chaboz, M.C. Hoener, M.E. Liechti, Pharmacological characterization of designer cathinones in vitro, Br. J. Pharmacol. 168 (2) (2013) 458–470, https://doi.org/10.1111/j.1476-5381.2012.02145.x.
[11] M. Coppola, R. Mondola, 3,4-methylenedioxypyrovalerone (MDPV): chemistry, pharmacology and toxicology of a new designer drug of abuse marketed online, Toxicol. Lett. 208 (1) (2012) 12–15, https://doi.org/10.1016/j.toxlet.2011.10.002.
[12] A. Namera, M. Kawamura, A. Nakamoto, T. Saito, M. Nagao, Comprehensive review of the detection methods for synthetic cannabinoids and cathinones, Forensic Toxicol. 33 (2) (2015) 175–194, https://doi.org/10.1007/s11419-015-0270-0.
[13] Y. Abiedalla, K. Abdel-Hay, J. DeRuiter, C.R. Clark, Differentiation of cyclic tertiary amine cathinone derivatives by product ion electron ionization mass spectrometry, Rapid Commun. Mass Spectrom. 30 (6) (2016) 763–772, https://doi.org/10.1002/rcm.7491.
[14] D. Zuba, Identification of cathinones and other active components of 'legal highs' by mass spectrometric methods, Trends Anal. Chem. 32 (2012) 15–30, https://doi.org/10.1016/j.trac.2011.09.009.
[15] E. Fornal, Identification of substituted cathinones: 3,4-Methylenedioxy derivatives by high performance liquid chromatography-quadrupole time of flight mass spectrometry, J. Pharmaceut. Biomed. Anal. 81–82 (2013) 13–19, https://doi.org/10.1016/j.jpba.2013.03.016.
[16] P. Jankovics, A. Varadi, L. Tolgyesi, S. Lohner, J. Nemeth-Palotas, H. Koszegi-Szalai, Identification and characterization of the new designer drug 4'-methylethcathinone (4-MEC) and elaboration of a novel liquid chromatography-tandem mass spectrometry (LC-MS/MS) screening method for seven different methcathinone analogs, Forensic Sci. Int. 210 (2011) 213–220, https://doi.org/10.1016/j.forsciint.2011.03.019.
[17] S. Matsuta, M. Katagi, H. Nishioka, H. Kamata, K. Sasaki, N. Shima, T. Kamata, A. Miki, M. Tatsuno, K. Zaitsu, K. Tsuboi, H. Tsuchihashi, K. Suzuki, Structural characterization of cathinone-type designer drugs by EI mass spectrometry, Jpn. J. Forensic Sci. Technol. 19 (2) (2014) 77–89.
[18] C. Sauer, F.T. Peters, C. Haas, M.R. Meyer, G. Fritschi, H.H. Maurer, New designer drug alpha-pyrrolidinovalerophenone (PVP): studies on its metabolism and toxicological detection in rat urine using gas chromatographic/mass spectrometric techniques, J. Mass Spectrom. 44 (6) (2009) 952–964, https://doi.org/10.1002/jms.1571.
[19] Y. Abiedalla, J. DeRuiter, C.R. Clark, G.C.–M.S., GC–MS/MS and GC-IR differentiation of carbonyl modified analogues of MDPV, Forensic Chem. 3 (2017) 58–68, https://doi.org/10.1016/j.forc.2016.11.002.
[20] K. Hasegawa, O. Suzuki, A. Wurita, K. Minakata, I. Yamagishi, H. Nozawa, K. Gonmori, K. Watanabe, Postmortem distribution of α-pyrrolidinovalerophenone and its metabolite in body fluids and solid tissues in a fatal poisoning case measured by LC–MS–MS with the standard addition method, Forensic Toxicol. 32 (2) (2014) 225–234, https://doi.org/10.1007/s11419-014-0227-8.
[21] M.J. Swortwood, K.N. Ellefsen, A. Wohlfarth, X. Diao, M. Concheiro-Guisan, R. Kronstrand, M.A. Huestis, First metabolic profile of PV8, a novel synthetic cathinone, in human hepatocytes and urine by high-resolution mass spectrometry, Anal. Bioanal. Chem. 408 (18) (2016) 4845–4856, https://doi.org/10.1007/s00216-016-9599-4.
[22] O.J. Pozo, M. Ibanez, J.V. Sancho, J. Lahoz-Beneytez, M. Farre, E. Papaseit, R. de la Torre, F. Hernandez, Mass spectrometric evaluation of mephedrone in vivo human metabolism: identification of phase I and phase II metabolites, including a novel succinyl conjugate, Drug Metab. Dispos. 43 (2) (2015) 248–257, https://doi.org/10.1124/dmd.114.061416.
[23] M. Ibanez, O.J. Pozo, J.V. Sancho, T. Orengo, G. Haro, F. Hernandez, Analytical strategy to investigate 3,4-methylenedioxypyrovalerone (MDPV) metabolites in consumers' urine by high-resolution mass spectrometry, Anal. Bioanal. Chem. 408 (1) (2016) 151–164, https://doi.org/10.1007/s00216-015-9088-1.
[24] D. Fabregat-Safont, X. Carbón, C. Gil, M. Ventura, J.V. Sancho, F. Hernández, M. Ibáñez, Reporting the novel synthetic cathinone 5-PPDI through its analytical characterization by mass spectrometry and nuclear magnetic resonance, Forensic Toxicol. 36 (2) (2018) 447–457, https://doi.org/10.1007/s11419-018-0422-0.
[25] Z. Qian, W. Jia, T. Li, Z. Hua, C. Liu, Identification of five pyrrolidinyl substituted cathinones and the collision-induced dissociation of electrospray-generated pyrrolidinyl substituted cathinones, Drug Test. Anal. 9 (5) (2017) 778–787, https://doi.org/10.1002/dta.2035.
[26] J.T. Davidson, E.L. Piacentino, Z.J. Sasiene, Y. Abiedalla, J. DeRuiter, C.R. Clark, G. Berden, J. Oomens, V. Ryzhov, G.P. Jackson, Identification of novel fragmentation pathways and fragment ion structures in the tandem mass spectra of protonated synthetic cathinones, Forensic Chem. 19 (2020) 100245, https://doi.org/10.1016/j.forc.2020.100245.
[27] L. Sleno, D. Volmer, Ion activation methods for tandem mass spectrometry,

J. Mass Spectrom. 39 (2004) 1091–1112.
[28] E. Fornal, Formation of odd-electron product ions in collision-induced fragmentation of electrospray-generated protonated cathinone derivatives: aryl alpha-primary amino ketones, Rapid Commun. Mass Spectrom. 27 (16) (2013) 1858–1866, https://doi.org/10.1002/rcm.6635.
[29] E. Fornal, Study of collision-induced dissociation of electrospray-generated protonated cathinones, Drug Test. Anal. 6 (2014) 705–715, https://doi.org/10.1002/dta.1573.
[30] S.A. McLuckey, D.E. Goeringer, Slow heating methods in tandem mass spectrometry, Int. J. Mass Spectrom. 32 (1997) 461–474.
[31] J. Mitchell Wells, S.A. McLuckey, Collision-Induced dissociation (CID) of peptides and proteins, in: Methods in Enzymology, 2005, pp. 148–185.
[32] A.H. Beckett, G.R. Jones, D.A. Hollingsbee, Degradation of (-)-ephedrine in solution and during extraction with diethyl ether, J. Pharm. Pharmacol. 30 (1978) 15–19.
[33] J. DeRuiter, L. Hays, A. Valaer, C.R. Clark, Methcathinone and designer drug analogs: synthesis, stereochemical analysis, and analytical properties, J. Chromatogr. Sci. 32 (1994) 552–564.
[34] S. Kerrigan, M. Savage, C. Cavazos, P. Bella, Thermal degradation of synthetic cathinones: implications for forensic toxicology, J. Anal. Toxicol. 40 (1) (2016) 1–11, https://doi.org/10.1093/jat/bkv099.
[35] F. Westphal, T. Junge, P. Rosner, G. Fritschi, B. Klein, U. Girreser, Mass spectral and NMR spectral data of two new designer drugs with an alpha-aminophenone structure: 4'-methyl-alpha-pyrrolidinohexanophenone and 4'-methyl-alpha-pyrrolidinobutyrophenone, Forensic Sci. Int. 169 (2007) 32–42, https://doi.org/10.1016/j.forsciint.2006.07.024.
[36] F. Westphal, T. Junge, P. Rosner, F. Sonnichsen, F. Schuster, Mass and NMR spectroscopic characterization of 3,4-methylenedioxypyrovalerone: a designer drug with alpha-pyrrolidinophenone structure, Forensic Sci. Int. 190 (2009) 1–8, https://doi.org/10.1016/j.forsciint.2009.05.001.
[37] J.D. Power, S.D. McDermott, B. Talbot, J.E. O'Brien, P. Kavanagh, The analysis of amphetamine-like cathinone derivatives using positive electrospray ionization with in-source collision-induced dissociation, Rapid Commun. Mass Spectrom. 26 (22) (2012) 2601–2611, https://doi.org/10.1002/rcm.6383.